# Bubble Breakup with Permanent Obstruction in an Asymmetric Microfluidic T-Junction

**Xiaoda Wang, Chunying Zhu, Taotao Fu, and Youguang Ma**
State Key Laboratory of Chemical Engineering, School of Chemical Engineering and Technology, Tianjin University, Tianjin 300072, China

*DOI 10.1002/aic.14704*
*Published online December 14, 2014 in Wiley Online Library (wileyonlinelibrary.com)*

*Bubble breakup with permanent obstruction in an asymmetric microfluidic T-junction is investigated experimentally. The breakup process of bubbles can be divided into three stages: squeezing, transition, and pinch-off stages. In the squeezing stage, the thinning of the bubble neck is mainly controlled by the velocity of the fluid flowing into the T-junction, and the increase of the liquid viscosity can promote this process. In the transition stage, the minimum width of bubble neck decreases linearly with time. In the pinch-off stage, the effect of the velocity of the fluid flowing into the T-junction on the thinning of the bubble neck becomes weaker, and the increase of the liquid viscosity would delay this process. The evolution of the minimum width of the bubble neck with the remaining time before the breakup can be scaled by a power–law relationship. The bubble length has little influence on the whole breakup process of bubbles.* © 2014 American Institute of Chemical Engineers *AIChE J*, 61: 1081–1091, 2015
*Keywords: bubble, breakup, microfluidics, T-junction, confinement*

## Introduction

Over the last decades, microfluidic technique has been applied to various domains such as materials synthesis, crystallization, drug encapsulation, protein screening, and emulsification due to the controllability, smart, and small characteristics of microfluidic devices.[1–7] Bubbles and droplets are always encountered in the application of microfluidic technique. By using microfluidic technique, highly monodisperse bubbles or droplets can be generated, which is of critical importance for the related biological and chemical technologies.[8,9] Several basic microfluidic configurations such as T-junctions, flow-focusing, and coflowing junctions have been used successfully to generate highly monodispersed bubbles or droplets.[10–12]

However, some of the applications of the microfluidic technique need further adjusting the sizes of bubbles or droplets in microfluidic devices. The breakup of bubbles or droplets into two or more highly monodispersed daughter bubbles or droplets could be a potential approach. There are three typical microfluidic configurations for the breakup of bubbles or droplets: narrow constriction,[13] obstacle,[14] and T- (or Y-) junction.[15–19] Among them, the T- (or Y-) junction is the most common one.[15–26] Link et al.[15] pioneered to apply the symmetrical microfluidic T-junction to passively break large droplets into smaller ones. The application of the symmetrical T-junction is limited, as it can only tailor the mother bubbles or droplets into two smaller ones with the same sizes. The asymmetrical T-junction could overcome this limitation and effectively improve the tailoring ability to control the sizes of the daughter bubbles or droplets, as the mother bubbles or droplets would breakup into two smaller daughter ones with different sizes in such junctions. Several methods are used to manipulate the asymmetry of the T-junction. By adjusting the length ratio of the two daughter arms of the T-junction, Link et al.[15] could control the volume ratio of the two daughter droplets. However, when the volume ratio of the two daughter droplets is large, this method needs greatly increasing the length of the microchannel. To overcome this drawback, Samie et al.[19] controlled the volume ratio of the two daughter droplets by adjusting the width ratio of the two daughter arms. Differently, Yamada et al.[18] tuned the volume ratio of the two daughter droplets by continuously introducing "tuning flow" into one of the daughter arms of the Y-junction. Moreover, some more complicated T-junction structures were also implemented to break bubbles and drops into smaller ones.[27,28]

To better control the bubble or droplet behaviors in the T-junction, we need first to understand the breakup mechanism of bubbles or droplets in such junctions. Tracing the dynamic process of the bubble or droplet neck is an effective and intuitive method to understand the mechanism for bubble or droplet breakup.[29] Leshansky et al.[24] analyzed theoretically the droplet breakup with permanent obstruction in a symmetric T-junction according to a simple geometric structure of the interface shape and Tanner's law of the local contact angle. They found that the variation of the minimum width of the droplet neck could be described by a power–law relation with an exponent of 3/7. The numerical simulation of Hoang et al.[26] indicated that the variation of the minimum width of the droplet neck was consistent with the theoretical prediction of Leshansky et al.[24] only during the inception stage of the breakup. After that, the droplet pinched off once the minimum width of the droplet neck

Correspondence concerning this article should be addressed to T. Fu at ttfu@tju.edu.cn and Y. Ma at ygma@tju.edu.cn

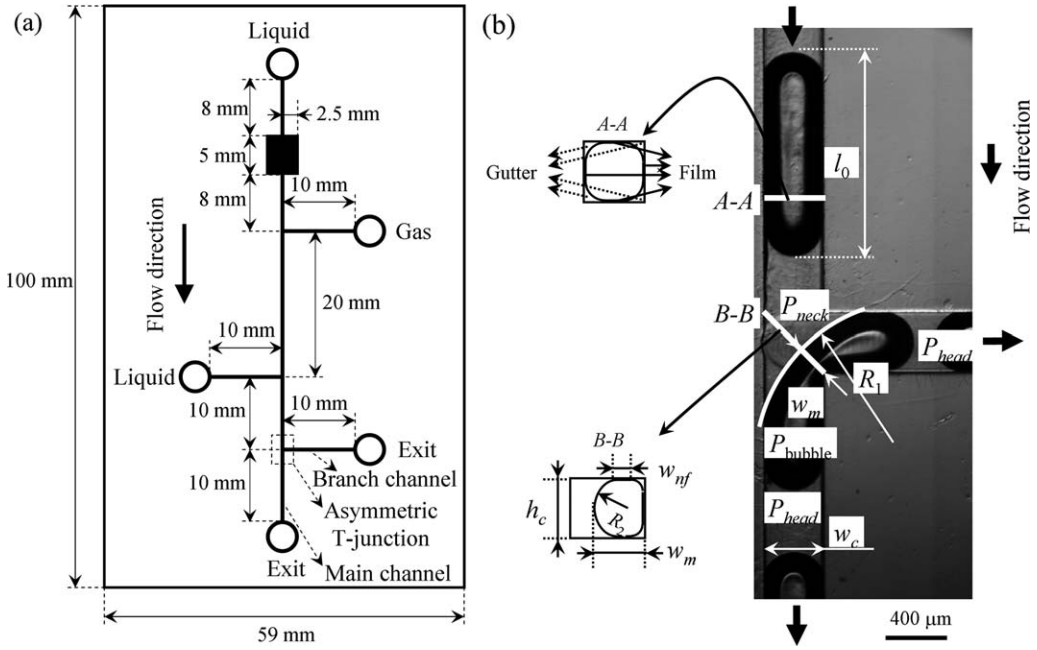


**Figure 1. (a) Schematic diagram of the microfluidic device. Both the lengths of the daughter channels of the asymmetric T-junction are 10 mm long. All the cross-sections of these microchannels are 400 μm (height) × 400 μm (width). The microfluidic device is about 100 mm long, 59 mm wide, and 21 mm high. (b) Sketch of the shape of a bubble arriving at the asymmetric T-junction and definitions of the parameters to characterize the breakup procedure of the bubble. $h_c$: the height of the cross-section of the square microchannel. $l_0$: the length of the bubble about to enter into the T-junction. $P_{bubble}$: the pressure in the breaking bubble. $P_{head}$: the pressure in the liquid near the head of the breaking bubble. $P_{neck}$: the pressure in the liquid near the neck of the breaking bubble. $R_1$ and $R_2$: the radius of curvature for the gas-liquid interface of the bubble neck in the direction parallel and perpendicular to the plane of the microfluidic device, respectively. $w_c$: the width of the cross-section of the square microchannel. $w_m$: the shortest distance from the gas-liquid interface of the bubble neck to the lower corner of the junction at the right hand. $w_{nf}$: The width of the film where the width of the neck of the bubble is minimum. Interface A–A: the cross-section (in the direction perpendicular to the plane of the microfluidic device) of the bubble moving in the feeding channel. Interface B–B: the cross-section (in the direction perpendicular to the plane of the microfluidic device) of the minimum width of the bubble neck.**

was smaller than a critical value. The critical minimum width of the droplet neck was related to the aspect ratio of the cross-section of microchannel, but not sensitive to the operating conditions and physical property of experimental fluid. Fu et al.[16] investigated experimentally the dynamics for three various types of symmetric bubble breakup in the microfluidic T-junction. By analyzing the breakup process, they found that the breakup mechanisms were different for various types of bubble breakup.

Several efforts have been devoted to the breakup mechanism of bubbles and droplets in symmetric T-junctions, but the breakup mechanism of bubbles in asymmetric T-junctions, which is helpful to predict the sizes of the daughter bubbles in the branching channels, has not been fully understood. In this work, the dynamics for bubble breakup with permanent obstruction in an asymmetric T-junction is studied experimentally, and the effects of the superficial velocity of the gas-liquid two-phase mixture, the viscosity of the continuous phase and the bubble length on the breakup of bubbles in such a junction are analyzed.

## Experimental Procedure

The experimental setup is sketched in Figure 1a. The gas phase and liquid phase meet each other in the first T-junction where bubbles are generated. The generated bubbles move downstream and arrive at the second T-junction where the liquid phase could be introduced to change the distance between sequential bubbles. After passing by the second T-junction, the bubbles move into the third T-junction where they can break up into two daughter bubbles. The daughter bubbles move through the arms of the T-junction and finally move out of the microfluidic device. Each arm of the asymmetric T-junction is 10 mm in length. This study is mainly concentrated on the bubble breakup in the third T-junction, as shown in Figure 1b. In this article, the asymmetric T-junction refers specially to the third T-junction. The microchannels were fabricated on a polymethyl methacrylate (PMMA) plate by a precision machine and sealed by another PMMA plate of equivalent size. Both the width and height of the cross-section of microchannel are 400 μm.

$N_2$ supplied by a $N_2$ cylinder was used as the dispersed phase. The gas flow rate was controlled by a high precision micrometering valve (Kofloc, Japan) and measured by a soap-film flowmeter. Liquid was pumped into the microchannel from a syringe by a syringe pump (Harvard Apparatus, PHD 22/2000). All the experiments were conducted at room temperature and atmospheric pressure. Different concentrations of glycerol (0–62 wt %) in deionized water were used as the continuous phase. The surfactant sodium dodecyl

**Table 1. Physical Properties of the Liquid Used in the Experiment**

| Liquid Phase | Surface Tension, $\sigma$ (mN m$^{-1}$) | Viscosity, $\mu$ (mPa s) | Density, $\rho$ (kg m$^{-3}$) |
|---|---|---|---|
| 0.3% SDS/water | 33 | 0.92 | 1000 |
| 0.3% SDS/35% glycerol | 32 | 2.60 | 1090 |
| 0.3% SDS/50% glycerol | 32 | 5.04 | 1140 |
| 0.3% SDS/62% glycerol | 31 | 9.56 | 1150 |

sulfate SDS (0.3 wt %) was added into the liquid to stabilize the bubble formation process. The surface tension was measured using a tensiometer, by the pendant drop technique on a Tracker apparatus (Dataphysics, Germany). An Ubbelohde capillary viscometer (Shanghai Qihang Glass Instruments Factory, China) was used to characterize the viscosity of the liquid phase. The density of the liquid phase was measured using a vibrating tuber density meter (Anton Paar DMA-4500-M, Austria). The properties of the experimental fluid were collected in Table 1.

In the experiment, a microscope equipped with a high speed camera (Redlake Motion Pro Y-5) was placed above the microfluidic device to capture the breakup process of bubble in the asymmetric T-junction. A cold fiber light (Philips 13629, Philips, Japan) placed under the microfluidic device, was used to illuminate the channel. The frame rates of the high speed camera were between 2000 and 10,000 frames per second.

Gas flow rate $Q_g$ is spanned between 2 and 60 mL h$^{-1}$, and liquid flow rate $Q_l$ between 2 and 90 mL h$^{-1}$. The corresponding capillary numbers $Ca = u\mu/\sigma$ ($u = (Q_g + Q_l)/w_c^2$; $u$ is the superficial velocity of the fluid flowing into the T-junction; $\mu$ and $\sigma$ are the viscosity and the surface tension of the liquid phase, respectively; $w_c$ is the width of the microchannel) ranges from 0.002 to 0.3. Reynolds number $Re = \rho w_c u/\mu$ ($\rho$ is the density of the liquid) ranges from 0.3 to 30. Weber number $We = CaRe = \rho w_c u^2/\sigma$ ranges from 0.0008 to 5.8.

## Results and Discussion

### *Breakup process for bubbles in the microfluidic T-junction*

The process for bubble breakup with permanent obstruction in the asymmetric T-junction includes three stages.[20] First, the forefront of the bubble expands in the asymmetric T-junction. Second, the forefront of the bubble moves forward in the two arms of the asymmetric T-junction simultaneously. Finally, the bubble breaks up into two different daughter ones driven by the continuous phase. In this work, the last stage is mainly studied to explore the mechanism for bubble breakup with permanent obstruction in the asymmetric T-junction.

A typical process for bubble breakup with permanent obstruction in the asymmetric T-junction is shown in Figure 2a. According to the evolution of the bubble neck, the breakup process can be further divided into three stages. In the first stage (0–7 ms), after the bubble completely enters into the asymmetric T-junction, the width of the bubble neck would continuously shrink under the squeezing of the continuous phase until the bubble neck detaches from the top- and bottom-wall at the end of this stage. The characteristic of this stage is that the outward convex bubble neck touches the channel walls by a very thin liquid film, and this process is named as the squeezing stage. In the second stage (8–12.5 ms), the width of the neck decreases gradually driven by the upstream continuous phase until the gas-liquid interface of the bubble neck becomes concave from convex. Differently from the first stage, the feature of the second stage is that the bubble detaches from the top- and bottom-wall of the microchannel near the bubble neck and forms two openings. This stage is named as the transition stage. In the third stage (14–15.6 ms), the concave neck of the bubble diminishes rapidly and finally ruptures, and this stage is named as the pinch-off stage.

To facilitate the research, several parameters are defined to quantify the breakup process of the bubbles, as shown in Figure 1b. $w_m$ is the shortest distance from the gas-liquid interface of the bubble neck to the lower corner of the junction at the right hand and $l_0$ is the length of the bubble before entering into the T-junction. $w_m$ and $l_0$ are normalized by the width of the microchannel $w_c$. $P_{bubble}$ is the pressure inside the breaking bubble. $P_{head}$ and $P_{neck}$ refer to the pressure of the continuous phase near the head and the neck of the breaking bubble, respectively. $R_1$ and $R_2$ are the radii of curvature for the gas-liquid interface of the bubble neck in

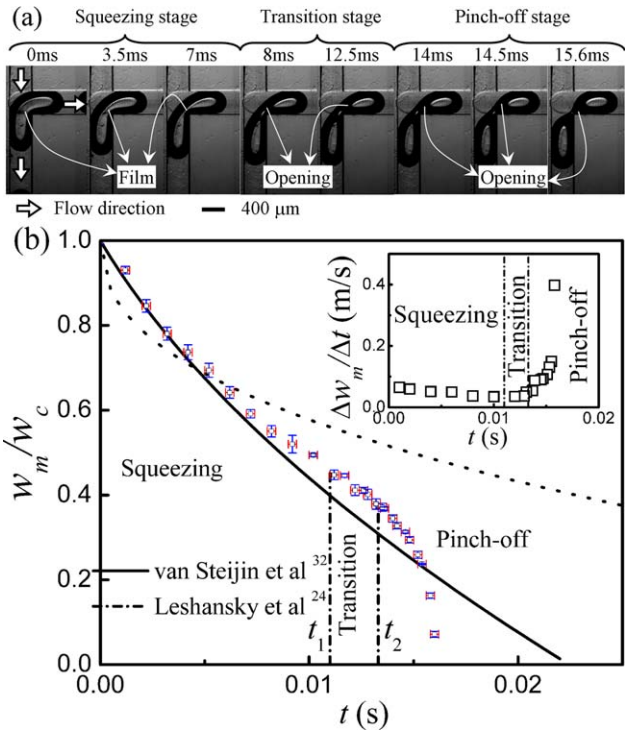


**Figure 2. (a) Evolution of the bubble breakup in the asymmetric microfluidic T-junction. (b) Temporal evolution of the minimum width of the neck for the breaking bubble in the asymmetric microfluidic T-junction. Inset: $\Delta w_m/\Delta t \sim t$. $t_1$: the beginning of the transition stage. $t_2$: the beginning of the pinch-off stage. Liquid phase: 35 wt % glycerol–water mixture with 0.3 wt % SDS. $l_0/w_c = 3.00$, $u = 0.05$ m/s. The short dash dot lines mark the time of $t_1$ and $t_2$.**

**[Color figure can be viewed in the online issue, which is available at wileyonline library.com.]**

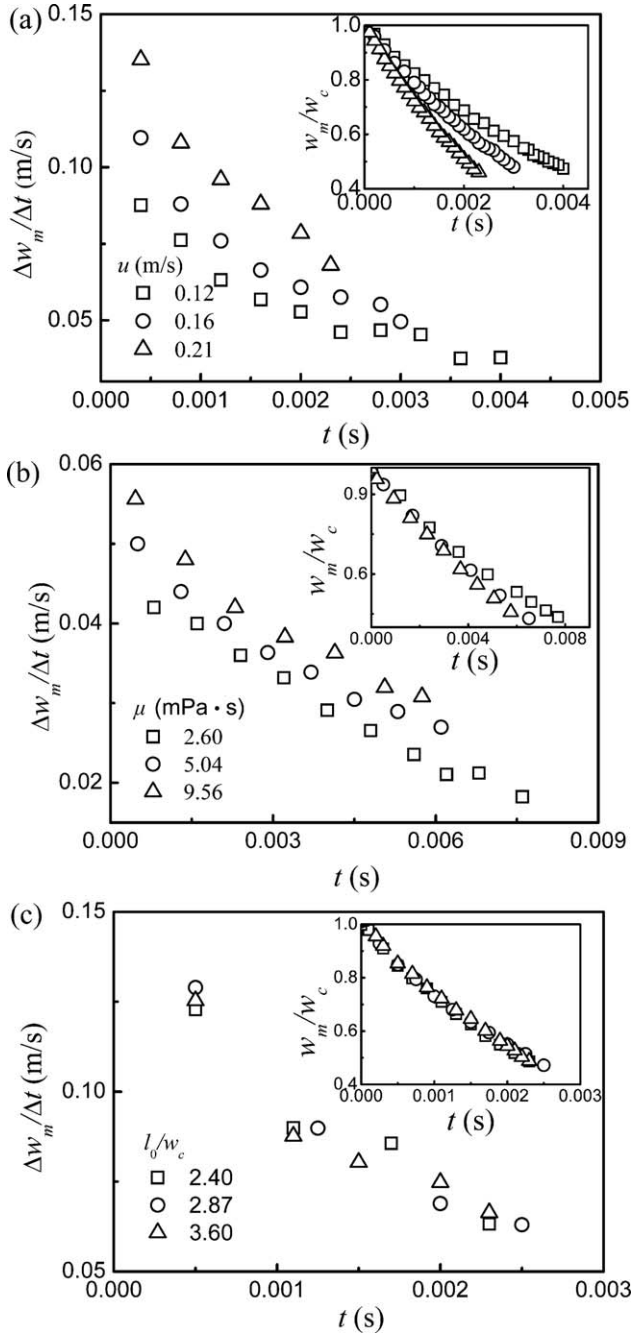


**Figure 3. Effects of the superficial velocity of fluid flowing into the T-junction, the viscosity of the continuous phase and the bubble length on the variation of the neck of the breaking bubble in the squeezing stage.**

**(a) Effect of the superficial velocity of fluid flowing into the T-junction. Liquid phase: water with 0.3 wt % SDS. $l_0/w_c = 3.00$. Inset: $w_m/w_c \sim t$. (b) Effect of the viscosity of the continuous phase. $l_0/w_c = 3.00$, $u = 0.07$ m/s. Inset: $w_m/w_c \sim t$. (c) Effect of the bubble length. Liquid phase: water with 0.3 wt % SDS. $u = 0.19$ m/s. Inset: $w_m/w_c \sim t$.**

the direction parallel and perpendicular to the plane of the microfluidic device, respectively.

The evaluation of $w_m/w_c$ with time is illustrated in Figure 2b. It could be clearly seen that the variation of $w_m/w_c$ with time behaves differently in different stages of the bubble breakup process. In the squeezing stage, $w_m/w_c$ decreases nonlinearly with time. The thinning rate of the bubble neck $\Delta w_m/\Delta t$ also declines with time as shown in the inset of Figure 2b. The squeezing stage needs the longest evolving time and the variation of $w_m/w_c$ in this stage is also the most greatest. Contrarily, the transition stage, in which $w_m/w_c$ decreases linearly with time, demands the shortest evolving time and the variation of $w_m/w_c$ in this stage is the smallest. In the pinch-off stage, $w_m/w_c$ descends nonlinearly with time, which is similar to the squeezing stage. However, the falling rate of the minimum width of the bubble neck $\Delta w_m/\Delta t$ increases rapidly with time as shown in the inset of Figure 2b. In addition, it is worth noting that in spite of approximate durations in the transition stage and the pinch-off stage, the change of $w_m/w_c$ in the pinch-off stage reaches almost up to four times than that in the transition stage. The evolution of $w_m/w_c$ with time shown in Figure 2b is a typical example in the present experiment, and the variation trend of $w_m/w_c$ would not vary with operating conditions and the properties of fluids.

### *Breakup dynamics of bubbles with permanent obstruction in the T-junction*

*The Squeezing Stage.* Figure 3 shows the effects of the superficial velocity of the fluid flowing into the T-junction $u$, the viscosity of the continuous phase μ, and the dimensionless bubble length $l_0/w_c$ on the evolution of bubble neck for the squeezing stage. The thinning rate of the bubble neck $\Delta w_m/\Delta t$ increases with the superficial velocity of the fluid flowing into the T-junction $u$ as shown in Figure 3a. The increase of the viscosity of the continuous phase would accelerate the thinning of bubble neck as shown in Figure 3b. The dimensionless bubble length $l_0/w_c$ has little effect on the variation of $w_m/w_c$ as shown in Figure 3c.

In the squeezing stage, the increase of the thinning rate of bubble neck with the superficial velocity of the fluid flowing into the T-junction could be attributed to the confinement effect of the microchannel walls. In the microchannel, the bubble usually becomes slender due to the confinement of channel walls, and the confined bubble touches each of the channel walls by means of a very thin liquid film. Four gutters are formed between the bubble and the four corners of the rectangle microchannel due to the effect of surface tension, as shown in the sketch of A–A cross-section in Figure 1b. In the square microchannel, the bubble accounts for about 90% cross-section area of the microchannel.[30] In the squeezing stage, a part of the continuous phase would squeeze the bubble neck to thin it, and another part would flow downward through the liquid films and gutters.[30,31] For the asymmetric T-junction, assuming no continuous phase flows through the liquid films and gutters, the dynamical evolution process of the neck of the confined bubble could be described by the following two equations[32]

$$\frac{dR_1}{dt} = \frac{16(Q_g + Q_l)}{h_c(4-\pi)(8R_1 + w_c\pi)} \tag{1}$$

$$w_m = R_1 - \sqrt{2}(R_1 - w_c) \tag{2}$$

Defining the time at $w_m/w_c = 1$ as inceptive one ($t = 0$, $w_m/w_c = 1$), we could obtain Eq. 3 by integrating Eq. 1

$$R_1 = -\frac{w_c\pi + \sqrt{[(8+\pi)w_c]^2 + 256(Q_g + Q_l)t/[(4-\pi)w_c]}}{8} \tag{3}$$

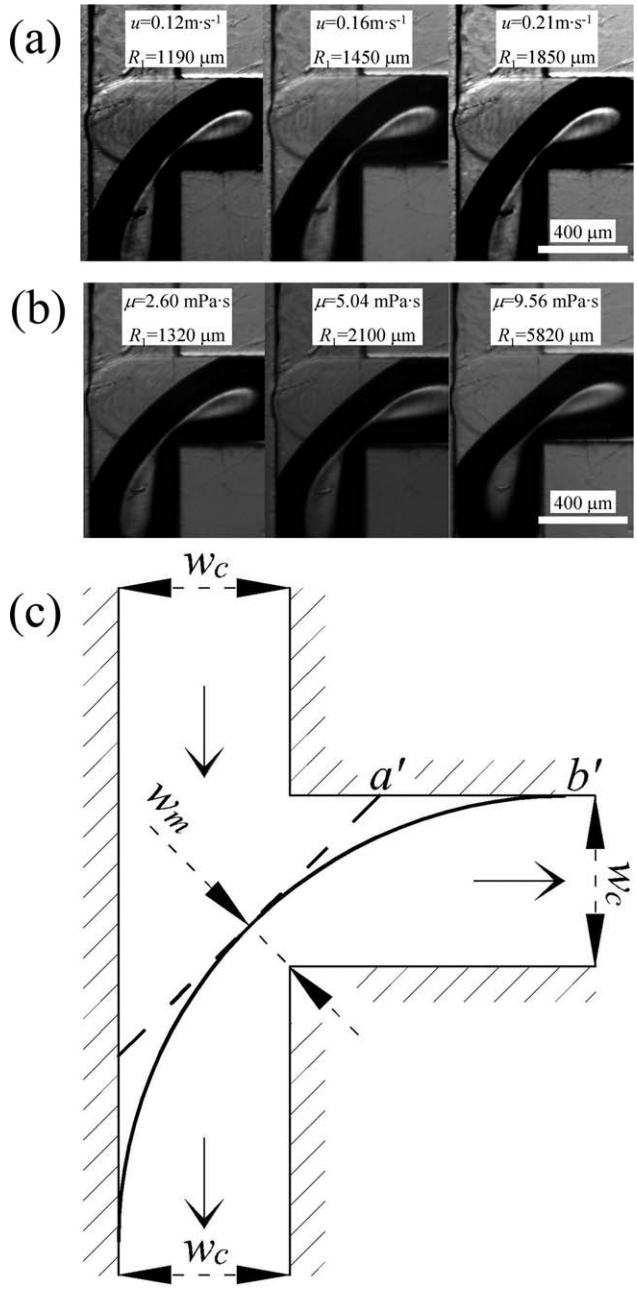


**Figure 4. Effects of the superficial velocity of fluid flowing into the T-junction, the viscosity of the continuous phase on the shape of the neck of the breaking bubble in the squeezing stage.**

**(a) Effect of the superficial velocity of fluid flowing into the T-junction. Liquid phase: water with 0.3 wt % SDS. $l_0/w_c = 3.00$, $w_m/w_c = 0.5$. (b) Effect of the viscosity of the continuous phase. $l_0/w_c = 3.00$, $u = 0.07$ m/s, $w_m/w_c = 0.5$. (c) Hypothetical shape for the gas-liquid interface of the bubble neck. a′: The bubble neck with larger $R_1$. b′: The bubble neck with smaller $R_1$. $R_1$: The radius of curvature for the gas-liquid interface of the bubble neck in the direction parallel to the plane of the microfluidic device.**

If no continuous phase flows through the liquid films and gutters, the evolution of the minimum width of the bubble neck with time could be attained by combining Eqs. 2 and 3, as shown in Figure 2a (the solid line). In the squeezing stage, the calculated widths of bubble neck are slightly smaller than the experimental ones. It means that most of the continuous phase was blocked and accordingly squeezed the bubble neck. Therefore, this is the primary reason why the thinning rate of the bubble neck increases with the superficial velocity of the fluid flowing into the T-junction.

In the squeezing stage, the increase of the viscosity of the continuous phase accelerates the thinning rate of the bubble neck by changing the shape of the gas-liquid interface of the bubble neck, as the shear force acted on the bubble neck is augmented with the increase of the viscosity of the continuous phase. This is similar to the effects of the superficial velocity of the fluid flowing into the T-junction on the bubble neck. The gas-liquid interface at the bubble neck would become less curved due to the increase of the shear force parallel to the interface, as shown in Figures 4a,b. At the same $w_m$, the less curved the gas-liquid interface is, the smaller the area of this interface is, as shown in Figure 4c. In the squeezing stage, if both the superficial velocity of the fluid flowing into the T-junction and the rate of the leakage are constant, the smaller the area of the gas-liquid interface is, the faster the advance speed of this interface is, that is, the faster the thinning of the bubble neck is. Therefore, the thinning of the bubble neck is accelerated by the decrease of the area of the gas-liquid interface owing to the increased viscous forces when the viscosity of the continuous phase is increased.

Our results suggest that the shear forces exerted on the bubble neck can deform the gas-liquid interface and that the deformation of the gas-liquid interface becomes more and more obvious with increasing the capillary number. However, these shear forces were not included in the force balance for bubble formation in a microfluidic T-junction in the squeezing regime, according to Garstecki et al.[10] They only considered the shear force acted on the gaseous thread invaded in the downstream channel of the T-junction, which has relative magnitude $l_0/d_{tun}$ ($d_{tun}$ is the thickness of the film between the bubble and the channel wall) in comparison with the squeezing force. Furthermore, this shear force is negligible as long as $l_0 >> d_{tun}$, for bubble formation in the T-junction in the squeezing regime. de Menech et al.[33] indicated that this shear force can not be neglected at relatively high capillary numbers. Christopher et al.[34] observed experimentally the squeezing-to-dripping transition for droplet formation in microfluidic T-junctions, and presented a scaling argument for predicting the droplet volume in this regime. However, this model overestimated the droplet size. The reason for the deviation was that this model only considered the shear force acted on the body of the dispersed phase in the downstream channel of the T-junction, neglecting the one acted on the neck of the dispersed phase in the T-junction. Therefore, the future studies should pay more attention to the shear force acted on the neck of the dispersed phase to have a better understanding on the mechanism for the breakup of bubble (or droplet) formation in the T-junction.

Although the leakage rate could also affect the thinning rate of the bubble neck, its effect could be neglected. The resistances to flow in the films and the gutters between the bubble and the channel walls decrease with the increase of the superficial velocity of the fluid flowing into the T-junction and the viscosity of the continuous phase due to the increase of the cross-section of the films and the gutters,[35,36] but decrease with the decrease of the bubble length due to the decrease of the lengths of the films and the gutters.

The reduction of the resistance results in the augment of the leakage rate, decelerating the thinning of the bubble neck. Differently from the influences of the superficial velocity of the fluid flowing into the T-junction and the viscosity of the continuous phase, the bubble length affects the thinning rate of the bubble neck only by changing the leakage rate. Therefore, the insignificant effect of the bubble length on the thinning rate of the bubble neck as shown in Figure 3c indicates that the effect of the leakage rate on the thinning rate of the bubble neck is negligible.

For the droplet breakup in the symmetric T-junction, Leshansky et al.[24] have proposed a correlation to describe the variation of the minimum width of the droplet neck with time: $w_m/w_c = 1 - 0.582\left(\frac{0.083}{Ca}\right)^{-1/7}\left(\frac{ut}{w_c}\right)^{3/7}$. The simulation of Hoang et al.[26] proved that the model can accurately predict the evolution of the droplet neck in the squeezing stage. Figure 2b indicates a comparison between our experimental results and the predicting values of the model by Leshansky et al.[24] It could be clearly found that there is a remarkable deviation between them. The deviation could be mainly attributed to the different driving forces for the breakup between the asymmetric and symmetric T-junction, which could be expressed as[27]

$$\Delta P_{dr} = \Delta P_{neck} + \Delta P_{head} = \sigma\left(\frac{1}{R_1} + \frac{1}{R_2} + \frac{4}{w_c}\right) \quad (4)$$

$\Delta P_{dr}$ is the driving force for the breakup of bubbles or droplets, and $\Delta P_{dr} = P_{neck} - P_{head}$; $\Delta P_{head}$ is the Laplace pressure at the head of the breaking bubble or droplets, and $\Delta P_{head} = P_{bubble} - P_{head}$; $\Delta P_{neck}$ is the Laplace pressure at the neck of the breaking bubble or droplets, and $\Delta P_{neck} = P_{neck} - P_{bubble}$. Both $\Delta P_{head}$ and $\Delta P_{neck}$ could be obtained by the Laplace equation. For the squeezing stage of the breakup in the symmetric T-junction, the neck of the bubble or droplet is always concave inward,[16,23] thus, $R_1$ and $R_2$ are positive values. However, for the asymmetric T-junction used in this study, the neck of the bubbles is convex outward in the inception period of the breakup, as shown in Figure 2a (0–7 ms), thus, $R_1$ and $R_2$ are negative values. This implies that the squeezing stage for the breakup of bubbles in the T-junction is also affected by the configuration of the junction.

*The Transition Stage*. The variations of $w_{mt}$ and $w_{mp}$ with the superficial velocity of the fluid flowing into the T-junction $u$ and the viscosity of the continuous phase $\mu$ are shown in Figure 5. $w_{mt}$ is the minimum width of bubble neck at the moment of detaching from the top and bottom walls. On the pictures captured by the high speed camera, the regime where the bubble has a close contact with the top and bottom walls appears bright, while the color of the regime where the bubble detaches from the top and bottom walls is black. Following this criterion, we could easily determine whether the bubble neck detaches from the top and bottom walls or not. It could be found from Figure 5 that $w_{mt}$ decreases with increasing the superficial velocity of the fluid flowing into the T-junction $u$ and the viscosity of the continuous phase $\mu$. Both the increase of the superficial velocity of the fluid flowing into the T-junction and the viscosity of the continuous phase could also make the gas-liquid interface of the bubble neck less curved by increasing the shear force acted on this interface, which is similar to the observation in the squeezing stage. As shown in the inset of Figure 1b, for the same minimum neck width, the less curved the gas-liquid interface of the bubble neck is, the higher the value of $w_{nf}$ ($w_{nf}$ is film width of the minimum width of the bubble neck) is. Since $w_{nf}$ and $w_m$ decrease simultaneously during the transition stage, the disappearance of the film of the minimum width of the bubble neck (or the detachment of the bubble neck from the top and bottom walls of the microchannel) would occur at lower values of $w_m$ for less curved gas-liquid interface of the bubble neck.

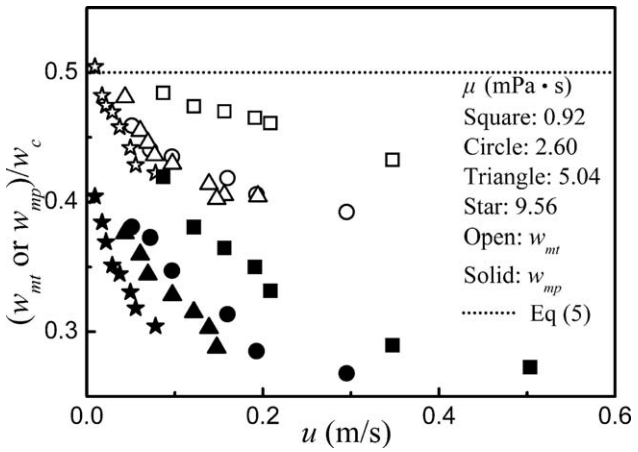


**Figure 5. Effects of the superficial velocity of the fluid flowing into the T-junction and the viscosity of the continuous phase on $w_{mt}$ and $w_{mp}$ for the bubble breakup at the T-junction.**

**$w_{mt}$: The minimum width of the bubble neck at the moment of detaching from the top and bottom walls of the microchannel. $w_{mp}$: The minimum width of the bubble neck when the shape of the bubble neck becomes from concave outward to convex inward.**

$w_{mp}$ is the minimum width of bubble neck when the shape of the bubble neck becomes from concave outward to convex inward. The affecting regulation of the superficial velocity of the fluid flowing into the T-junction and the viscosity of the continuous phase on $w_{mp}$ could be found in Figure 5, which accords well with that for droplet formation in microfluidic T-junction.[37,38] According to Glawdel et al.,[38] only when $Ca \to 0$, $w_{mp}$ could approach the predicted value by van Steijn et al.[32]

$$w_{mp} = \frac{w_c h_c}{w_c + h_c} \quad (5)$$

where $h_c$ is the height of the microchannel. The bubble breakup as $Ca \to 0$ has not been observed in our experiments, but it seems to be logical to assume that $w_{mp}$ would approach the value predicted by Eq. 5 when both the superficial velocity of the fluid flowing into the T-junction and the viscosity of continuous phase tend to 0 ($Ca \to 0$), by extrapolating the variation of $w_{mp}$ shown in Figure 5. It is noteworthy that the pinch-off stage occurs when the minimum width of the bubble neck is equal to the height of the microchannel for the bubble formation in a flow-focusing device.[39] However, this argument needs to be validated by varying capillary numbers. It may be reasonable that the occurrence of this stage depends not only on the capillary number but also on the configuration of the microchannel.

The effects of the superficial velocity of the fluid flowing into the T-junction, the viscosity of the continuous phase and the dimensionless bubble length on the thinning rate of the bubble neck during transition stage are shown in Figure

6. It could be seen from Figure 6 that the thinning rate of the bubble neck increases with the superficial velocity of the fluid flowing into the T-junction and the viscosity of the continuous phase, but the effect of the dimensionless bubble length on the thinning of the bubble neck is nearly negligible. This is quite similar to those in the squeezing stage. In the transition stage, two up- and down- openings appear between the bubble and the walls due to the detachment of bubble neck from top and bottom walls of the microchannels, as shown in Figure 2a. The continuous phase could flow toward the four gutters opposite to the feeding channel between the bubble and channel through the two openings. Compared to the squeezing stage, the liquid flowing through gutters would be increased in the transition stage. As shown in Figure 2b, at the beginning of the pinch-off stage $t_2$, the deviation of the minimum width of the bubble neck between the calculated values from Eqs. 2 and 3, and the experimental data are not noticeable. It indicates that the leakage of the liquid in the transition stage remains still not remarkable in spite of the appearance of the two openings.

In principle, in the transition stage, the thinning rate of the bubble neck are dominated essentially by the superficial velocity of the fluid flowing into the T-junction and the viscosity of the continuous phase, regardless of the dimensionless bubble length. Therefore, we could correlate the normalized thinning rate of the bubble neck $\Delta(w_m/w_c)/\Delta(t/T_c)$ to dimensionless numbers such as capillary number $Ca = u\mu/\sigma$ and Reynolds number $Re = \rho w_c u/\mu$ by means of the multiple regression method

$$\Delta(w_m/w_c)/\Delta(t/T_c) = 0.44 Ca^{0.57} Re^{0.44} \sim u^{1.01}\mu^{0.13} \quad (6)$$

The capillary time $T_c$ is defined as $T_c = (\rho w_c^3/\sigma)^{1/2}$.[29] The mean relative deviation of the correlation is 3.99%. By comparing the exponents of $u$ and $\mu$ in Eq. 6, it could be found that the influence of the superficial velocity of the fluid flowing into the T-junction on the thinning rate of the bubble neck is more significant than that of the viscosity of the continuous phase. It is noteworthy that the results of our experiments are different from those observed by Garstecki et al.,[40] who found that the collapse rate depends only on the superficial velocity flowing into the T-junction, but in accord with the conclusion of Fu et al.,[41] as the collapse of bubbles is affected by the confinement of the microchannel on the flowing fluid.[41] It is interesting to note that the thinning rates of the bubble neck measured in our experiments are 1–2 orders of magnitude smaller than the speed calculated by the classical theory of capillary breakup. This is similar to the results of Garstecki et al.[40] and Fu et al.[41] It suggests that, the bubble interface is stable against the capillary instability during the transition stage.[40]

*The Pinch-Off Stage*. From Figure 2b, it could be easily found that the variation trend of $w_m/w_c$ with time in pinch-off stage is much different from these in the previous two stages. The thinning rate of the bubble neck diminishes gradually with time in the squeezing stages until near a constant in the transition stage. Conversely, it increases rapidly with time in the pinch-off stage.

To better understand the driving mechanism for the pinch-off stage, the variations of the driving force $\Delta P_{dr}$ and the minimum width of the bubble neck $w_m$ with time were analyzed as shown in Figures 7 and 8. Figure 7a shows the variation of $\Delta P_{dr}$ with time. The $\Delta P_{dr}$ at different time could be calculated from Eq. 4. The value of $R_1$ in this equation could be extracted from the pictures captured by the high speed camera. Since the shape of the longitudinal cross-section of the minimum width of the bubble neck could not be directly visualized, we make several assumptions about the contour line of this cross-section to calculate $R_2$ as shown in Figure 7b. In the squeezing stage, the contour line that does not touch the microchannel walls is assumed as an arc, thus $R_2^2 = (R^2 - b)^2 + (h_c/2)^2$, where $b$ is the height of the arc. The value of $b$ could be obtained from the pictures captured by the high speed camera. On these pictures, the regime where the bubble detaches from the top and bottom walls appears black, and is different from the regime in close contact with the bubble. In the transition and pinch-off stages, the contour line of the A–A cross-section is assumed as a circle, thus $R_2 = w_c/2$. It could be seen from Figure 7a that: in the squeezing stage, the value of $\Delta P_{dr}$ is positive and increases slightly with time; in the pinch-off stage, the value of $\Delta P_{dr}$ becomes negative and decreases rapidly. The change of the sign of $\Delta P_{dr}$ implies the change of the direction of the driving force. The variation of $\Delta P_{dr}$ is similar to that for the bubble formation in a microfluidic T-junction reported by van Steijn et al.[32] They thought that the change of the direction of the driving force reserved the liquid near the bubble head toward

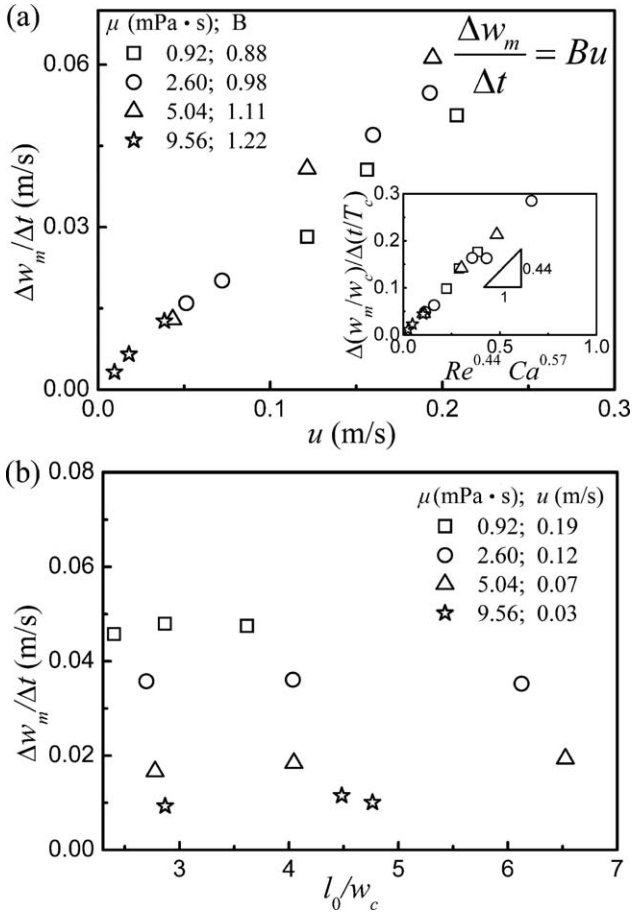


**Figure 6. Effects of the superficial velocity of the fluid flowing into the T-junction, the viscosity of the continuous phase and the bubble length on the thinning rate of the neck for bubble breakup in the transition stage.**

**(a) Effects of the superficial velocity of the fluid flowing into the T-junction and the viscosity of the continuous phase. Inset: $\Delta(w_m/w_c)/\Delta(t/T_c) \sim Re^{0.44}Ca^{0.57}$. (b) Effect of the bubble length.**

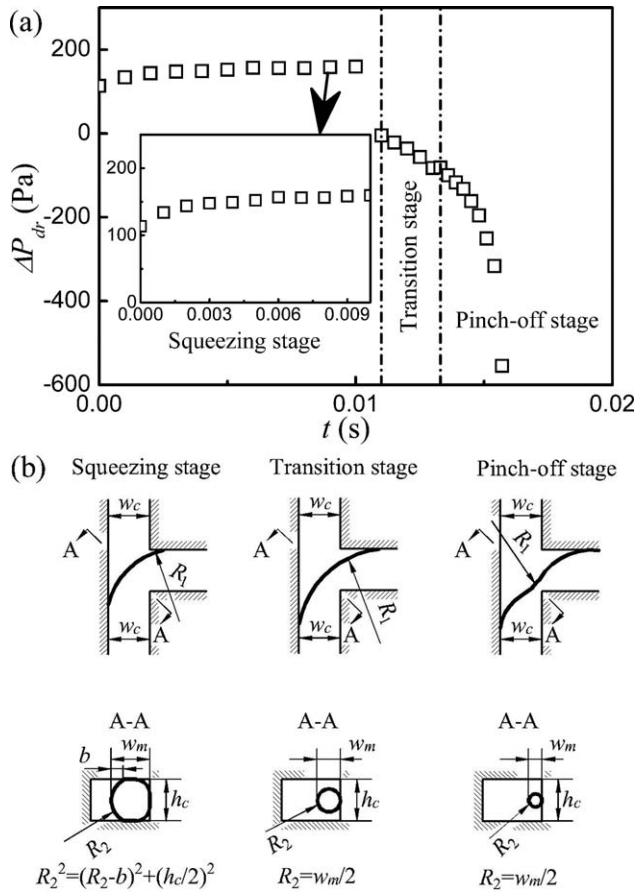


**Figure 7. (a) Temporal evolution of the pressure difference between the bubble head and the bubble neck. Inset: the amplification of the temporal evolution of the pressure difference in the squeezing stage. The short dash dot lines: the transitions between various stages for bubble breakup. Liquid phase: 35 wt % glycerol–water mixture with 0.3 wt % SDS. $l_0/w_c = 3.00$, $u = 0.05$ m/s. (b) Definition of $R_1$ and $R_2$ for each stage. $R_1$ and $R_2$: the radius of curvature for the gas-liquid interface of the bubble neck in the direction parallel and perpendicular to the plane of the microfluidic device, respectively. Interface A–A: the cross-section of the minimum width of the bubble neck.**

the bubble neck, triggering the pinch-off for bubble formation at the T-junction. According to the analysis on $\Delta P_{dr}$, it seems that the pinch-off mechanism for bubble breakup is similar to that for bubble formation in a microfluidic T-junction.[32]

The variation of the minimum width of the bubble neck $w_m$ with the remaining time $(T-t)$ is shown in Figure 8. It could be clearly seen that the pinch-off stage is a self-similar thinning process.[42–46] The variation of the minimum width of the bubble neck $w_m$ with the remaining time $(T-t)$ before the final pinch-off could be described by a power–law relationship with an exponent of 1/3: $w_m \sim (T-t)^{1/3}$. The exponent 1/3 is independent of the superficial velocity of the fluid flowing into the T-junction, the viscosity of the continuous phase and the bubble length. The similar power–law relationship between the minimum width of the bubble neck and the remaining time was also observed for the formation of bubbles in the microfluidic flow-focusing devices, but the value of the exponent varied with the variations of the dimensions of the microchannels and the operating conditions.[39,47,48] Furthermore, it could be found from Figure 8 that the variation of $w_m/w_c$ is moderately affected by the superficial velocity of the fluid flowing into the T-junction

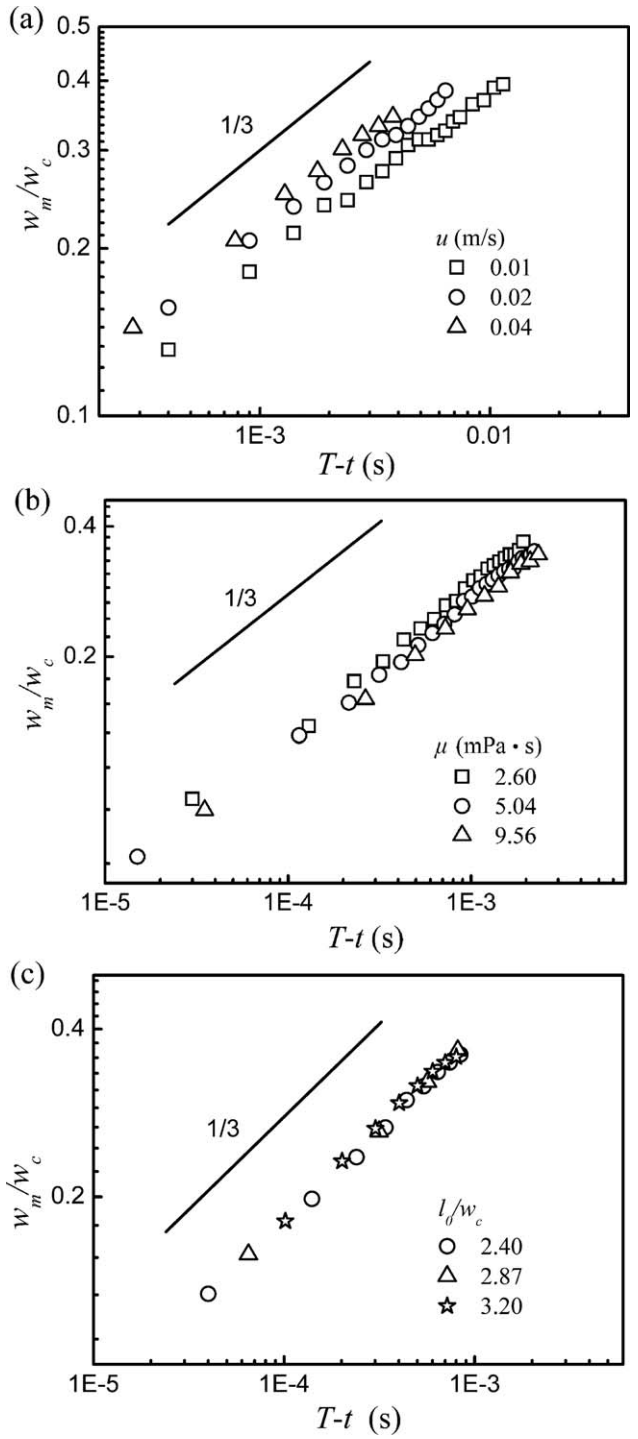


**Figure 8. Scaling of $w_m$ in function of the remaining time $(T-t)$ for the pinch-off stage.**

**(a) Effect of the superficial velocity of the fluid flowing into the T-junction. $l_0/w_c = 3.00$. Liquid phase: 62 wt % glycerol–water mixture with 0.3 wt % SDS. (b) Effect of the viscosity of the continuous phase. $l_0/w_c = 3.00$, $u = 0.07$ m/s. (c) Effect of the bubble length. Liquid phase: water with 0.3 wt % SDS. $u = 0.19$ m/s.**

and the viscosity of the continuous phase and nearly irrelevant to the bubble length in the pinch-off stage. A scaling law could be obtained to predict $w_m/w_c$ by taking the influence of the superficial velocity of the fluid flowing into the T-junction and viscosity of the continuous phase into account

$$w_m/w_c = 0.53Re^{0.14}\left(\frac{T-t}{T_c}\right)^{1/3} \quad (7)$$

The mean relative deviation of the correlation is 2.61%. From Eq. 7, we could see that the pinch-off rate of the bubble neck increases with the superficial velocity of the fluid flowing into the T-junction. It means that the inertia of the upstream fluid also has effect on the pinch-off stage for bubble breakup in the asymmetric T-junction. In addition, Eq. 7 indicates that the pinch-off rate of the bubble neck decreases with the increase of the viscosity of the continuous phase.

### *The breakup time*

The analyses for the time of the bubble breakup with permanent obstruction in the T-junction are illustrated in Figure 9. From Figures 9a,b, we could find that: (1) the breakup time of the bubble rapidly reduces with the increase of the superficial velocity of the fluid flowing into the T-junction, especially as it is smaller than 0.1 m $s^{-1}$; (2) the effects of the viscosity of the continuous phase and the bubble length on the breakup time of bubbles are nearly negligible. The observable effect of the superficial velocity of the fluid flowing into the T-junction on the breakup time is attributed to the fact that the time occupied by the squeezing and transition stages, both of which are dominated by the fluid flowing into the T-junction, accounts for more than 80% of the total breakup time of the bubble, as shown in Figure 9c. There are two reasons for the unremarkable effect of the viscosity of the continuous phase on the breakup time of the bubble. First, the effect of the viscosity of the continuous phase on the dynamics for the bubble breakup is not as noticeable as that of the superficial velocity of the fluid flowing into the T-junction. Second, the increase of the viscosity of the continuous phase could promote the thinning of the bubble neck for the squeezing and transition stages but decelerate it for the pinch-off stage. The competitive results of the two opposite actions are compromise. Furthermore, the breakup time of the bubble can be expressed as: $T/T_c = 2(uT_c/w_c)^{-0.93}$ as shown in Figure 9a. The average relative deviation of the correlation is 7.67%.

## Conclusion

To conclude, the bubble breakup with permanent obstruction is investigated experimentally, and the effects of the superficial velocity of the fluid flowing into the T-junction, the viscosity of the continuous phase and the bubble length on breakup dynamics of bubbles are studied systematically. The breakup process of bubbles in the T-junctions could be divided into three stages: the squeezing stage, the transition stage, and the pinch-off stage. In the squeezing stage, the thinning rate of the bubble neck decreases nonlinearly with time. In the transition stage, the minimum width of the bubble neck decreases linearly with time and is related to the capillary number $Ca$ and the Reynolds number $Re$: $\Delta(w_m/w_c)/\Delta(t/T_c) = 0.44Ca^{0.57}Re^{0.44}$. However, whether this relationship is applicable or not for the rectangular microchannels and the square microchannels with different

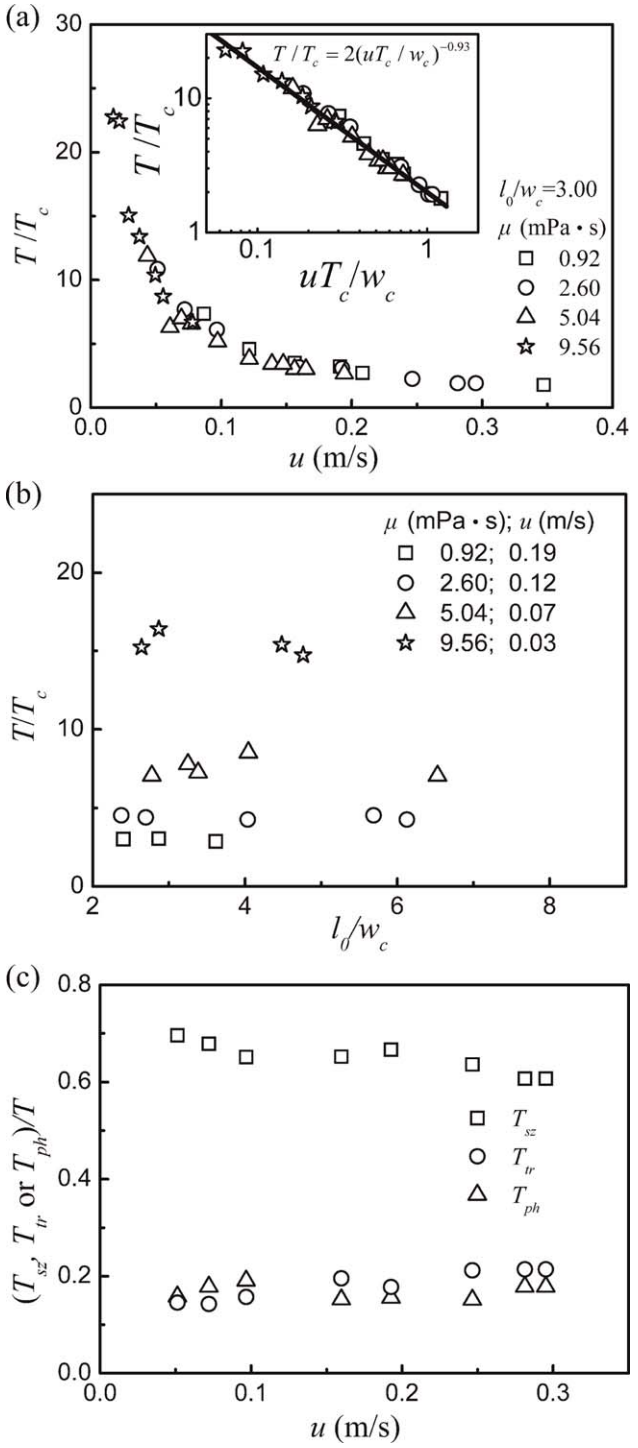


**Figure 9. (a) and (b) Effects on the breakup time of bubble. (a) The superficial velocity of the fluid flowing into the T-junction and the viscosity of the continuous phase. Inset: log ($T/T_c$) ~ log $u$. (b) The bubble length. (c) Proportions of time occupied by the squeezing, transition, and pinch-off stage respectively in the entire period of bubble breakup. Liquid phase: 35 wt % glycerol–water mixture with 0.3 wt % SDS. $l_0/w_c = 3.00$.**

dimensions still needs to be further verified. In the pinch-off stage, the thinning rate of the bubble neck increases nonlinearly with time, and the variation of the minimum width of the bubble neck with the remaining time could be scaled as a power–law relationship: $w_m/w_c=0.53Re^{0.14}\left(\frac{T-t}{T_c}\right)^{1/3}$. Nevertheless, how do the dimension and the shape of the cross-section of the microchannel affect the exponent for the power–law relation for the minimum width of the bubble neck and the dimensionless remaining time should be paid more attention in the further study. During the whole breakup process, the superficial velocity of the fluid flowing into the T-junction is a key impacting factor on the thinning rate of the bubble neck, and its augment could promote this process. In the pinch-off stage, though the effect of the superficial velocity of the fluid flowing into the T-junction becomes weaker, but remains nonignorable. Compared to the superficial velocity of the fluid flowing into the T-junction, the viscosity of the continuous phase has also somewhat influence on the thinning rate of the bubble neck. The increase of the liquid viscosity could accelerate the thinning of the bubble neck in the squeezing stage and transition stage, but decelerate that in the pinch-off stage. The bubble length has no effect on the bubble breakup for all of the three stages of. Furthermore, the breakup time of bubble is primarily dominated by the superficial velocity of the fluid flowing into the T-junction and can be expressed as: $T/T_c=2(uT_c/w_c)^{-0.93}$. This study enriches our understanding of the mechanism for bubble breakup in the microfluidic T-junction, and could serve as theoretical basis for predicting the sizes of the daughter bubbles in the asymmetrical microfluidic T-junction.[17]

## Acknowledgments

The financial supports for this project from the National Natural Science Foundation of China (21106093 and 21276175), the Tianjin Natural Science Foundation (13JCQNJC05500), and the Program of Introducing Talents of Discipline to Universities (B06006) are gratefully acknowledged.

## Notation

$b$ = height of the arc in Figure 7b, m.
$d_{tun}$ = thickness of the tunnels between the bubble and the walls of microchannel, m.
$h_c$ = height of the cross-section of the microchannel, m.
$l_0$ = length of the bubble about to enter into the T-junction, m.
$\Delta P_{dr}$ = driving force for bubble breakup, Pa.
$\Delta P_{head}$ = Laplace pressure at the head of the breaking bubble, Pa.
$\Delta P_{neck}$ = Laplace pressure at the neck of the breaking bubble, Pa.
$P_{bubble}$ = pressure in the breaking bubble, Pa.
$P_{head}$ = pressure in the liquid near the neck of the breaking bubble, Pa.
$P_{neck}$ = pressure in the liquid near the neck of the breaking bubble, Pa.
$Q_g$ = volumetric flow rate of the gas phase, $m^3\ s^{-1}$
$Q_l$ = volumetric flow rate of the liquid phase, $m^3\ s^{-1}$.
$R_1$ = radius of curvature for the gas-liquid interface of the bubble neck in the direction parallel to the plane of the microfluidic device, m.
$R_2$ = radius of curvature for the gas-liquid interface of the bubble neck in the direction perpendicular to the plane of the microfluidic device, m.
$T$ = breakup time of bubble, s.
$T_c$ = capillary time, s.
$t$ = time, s.
$t_1$ = beginning of the transition stage, s.
$t_2$ = beginning of the pinch-off stage, s.
$u$ = superficial velocity of the fluid flowing into the T-junction, m $s^{-1}$.
$w_c$ = width of the cross-section of the microchannel, m.
$w_{nf}$ = width of the film of the minimum width of the bubble neck, m.
$w_m$ = shortest distance from the gas-liquid interface of the bubble neck to the lower corner of the junction at the right hand, m.
$w_{mp}$ = minimum width of the bubble neck when the shape of the bubble neck becomes from concave outward to convex inward, m.
$w_{mt}$ = minimum width of the bubble neck at the moment of detaching from the top and bottom walls of the microchannel, m.

### *Greek letters*

$\mu$ = viscosity of the liquid, mPa s.
$\rho$ = density of the liquid, kg $m^{-3}$.
$\sigma$ = surface tension of the liquid, mN $m^{-1}$.

### *Dimensionless groups*

$Ca$ = capillary number ($Ca = u\mu/\sigma$).
$Re$ = Reynolds number ($Re = \rho w_c u/\mu$).
$We$ = Weber number ($We = CaRe = \rho w_c u^2/\sigma$).

## Literature Cited

1. Agrestia JJ, Antipov E, Abate AR, Ahn K, Rowat AC, Baret J-C, Marquez M, Klibanov AM, Griffiths AD, Weitz DA. Ultrahigh-throughput screening in drop-based microfluidics for directed evolution. *Proc Natl Acad Sci USA*. 2010;107:4004–4009.
2. Huynh T, Sun B, Li L, Nichols KP, Koyner JL, Ismagilov RF. Chemical analog-to-digital signal conversion based on robust threshold chemistry and its evaluation in the context of microfluidics-based quantitative assays. *J Am Chem Soc*. 2013;135:14775–14783.
3. Kirby AE, Wheeler AR. Microfluidic origami: a new device format for in-line reaction monitoring by nanoelectrospray ionization mass spectrometry. *Lab Chip*. 2013;13:2533–2540.
4. Majedi FS, Hasani-Sadrabadi MM, Emami SH, Shokrgozar MA, VanDersarl JJ, Dashtimoghadam E, Bertsch A, Renaud P. Microfluidic assisted self-assembly of chitosan based nanoparticles as drug delivery agents. *Lab Chip*. 2013;13:204–207.
5. Marre S, Jensen KF. Synthesis of micro and nanostructures in microfluidic systems. *Chem Soc Rev*. 2010;39:1183–1202.
6. Whitesides GM. The origins and the future of microfluidics. *Nature*. 2006;442:368–373.
7. Xu S, Zhang Y, Jia L, Mathewson KE, Jang K-I, Kim J, Fu H, Huang X, Chava P, Wang R, Bhole S, Wang L, Na YJ, Guan Y, Flavin M, Han Z, Huang Y, Rogers JA. Soft microfluidic assemblies of sensors, circuits, and radios for the skin. *Science*. 2014;344:70–74.
8. Puigmarti-Luis J. Microfluidic platforms: a mainstream technology for the preparation of crystals. *Chem Soc Rev*. 2014;43:2253–2271.
9. Seemann R, Brinkmann M, Pfohl T, Herminghaus S. Droplet based microfluidics. *Rep Prog Phys*. 2012;75:016601.
10. Garstecki P, Fuerstman MJ, Stone HA, Whitesides GM. Formation of droplets and bubbles in a microfluidic T-junction-scaling and mechanism of break-up. *Lab Chip*. 2006;6:437–446.
11. Anna SL, Bontoux N, Stone HA. Formation of dispersions using "flow focusing" in microchannels. *Appl Phys Lett*. 2003;82:364–366.
12. Gañán-Calvo AM, Gordillo JM. Perfectly monodisperse microbubbling by capillary flow focusing. *Phys Rev Lett*. 2001;87:274501.
13. Rosenfeld L, Fan L, Yunhan Chen, Swoboda R, Tang SKY. Break-up of droplets in a concentrated emulsion flowing through a narrow constriction. *Soft Matter*. 2014;10:421–430.
14. Salkin L, Courbin L, Panizza P. Microfluidic breakups of confined droplets against a linear obstacle: the importance of the viscosity contrast. *Phys Rev E*. 2012;86:036317.
15. Link D, Anna S, Weitz D, Stone H. Geometrically mediated breakup of drops in microfluidic devices. *Phys Rev Lett*. 2004;92:054503.
16. Fu T, Ma Y, Funfschilling D, Li HZ. Dynamics of bubble breakup in a microfluidic T-junction divergence. *Chem Eng Sci*. 2011;66:4184–4195.
17. Fu T, Ma Y, Li HZ. Hydrodynamic feedback on bubble breakup at a T-junction within an asymmetric loop. *AIChE J*. 2014;60:1920–1929.
18. Yamada M, Doi S, Maenaka H, Yasuda M, Seki M. Hydrodynamic control of droplet division in bifurcating microchannel and its application to particle synthesis. *J Colloid Interf Sci*. 2008;321:401–407.

19. Samie M, Salari A, Shafii MB. Breakup of microdroplets in asymmetric T junctions. *Phys Rev E*. 2013;87:053003.
20. Wang X, Zhu C, Fu T, Ma Y. Critical lengths for the transition of bubble breakup in microfluidic T-junctions. *Chem Eng Sci*. 2014; 111:244–254.
21. de Menech M. Modeling of droplet breakup in a microfluidic T-shaped junction with a phase-field model. *Phys Rev E*. 2006;73: 031505.
22. Ménétrier-Deremble L, Tabeling P. Droplet breakup in microfluidic junctions of arbitrary angles. *Phys Rev E*. 2006;74:035303.
23. Jullien MC, Ching MJTM, Cohen C, Menetrier L, Tabeling P. Droplet breakup in microfluidic T-junctions at small capillary numbers. *Phys Fluids*. 2009;21:072001.
24. Leshansky AM, Afkhami S, Jullien MC, Tabeling P. Obstructed breakup of slender drops in a microfluidic T junction. *Phys Rev Lett*. 2012;108:264502.
25. Leshansky AM, Pismen LM. Breakup of drops in a microfluidic T junction. *Phys Fluids*. 2009;21:023303.
26. Hoang DA, Portela LM, Kleijn CR, Kreutzer MT, van Steijn V. Dynamics of droplet breakup in a T-junction. *J Fluid Mech*. 2013; 717:R4.
27. Song Y, Manneville P, Baroud CN. Local interactions and the global organization of a two-phase flow in a branching tree. *Phys Rev Lett*. 2010;105:134501.
28. Baudoin M, Song Y, Manneville P, Baroud CN. Airway reopening through catastrophic events in a hierarchical network. *Proc Natl Acad Sci USA*. 2013;110:859–864.
29. Basaran OA. Small-scale free surface flows with breakup: Drop formation and emerging applications. *AIChE J*. 2002;48: 1842–1848.
30. Wu Y, Fu T, Zhu C, Lu Y, Ma Y, Li HZ. Asymmetrical breakup of bubbles at a microfluidic T-junction divergence: Feedback effect of bubble collision. *Microfluidic Nanofluidic*. 2012;13: 723–733.
31. van Steijn V, Kreutzer MT, Kleijn CR. $\mu$-PIV study of the formation of segmented flow in microfluidic T-junctions. *Chem Eng Sci*. 2007; 62:7505–7514.
32. van Steijn V, Kleijn CR, Kreutzer MT. Flows around confined bubbles and their importance in triggering pinch-off. *Phys Rev Lett*. 2009;103:214501.
33. de Menech M, Garstecki P, Jousse F, Stone HA. Transition from squeezing to dripping in a microfluidic T-shaped junction. *J Fluid Mech*. 2008;595:141–161.
34. Christopher GF, Noharuddin NN, Taylor JA, Anna SL. Experimental observations of the squeezing-to-dripping transition in T-shaped microfluidic junctions. *Phys Rev E*. 2008;78:036317.
35. Thulasidas TC, Abraham MA, Cerro RL. Bubble-train flow in capillaries of circular and square cross section. *Chem Eng Sci*. 1995;50: 183–199.
36. Fries DM, Trachsel F, von Rohr PR. Segmented gas–liquid flow characterization in rectangular microchannels. *Int J Multiphase Flow*. 2008;34:1108–1118.
37. Glawdel T, Elbuken C, Ren CL. Droplet formation in microfluidic T-junction generators operating in the transitional regime. I. Experimental observations. *Phys Rev E*. 2012;85:016322.
38. Glawdel T, Elbuken C, Ren CL. Droplet formation in microfluidic T-junction generators operating in the transitional regime. II. Modeling. *Phys Rev E*. 2012;85:016323.
39. Dollet B, van Hoeve W, Raven J-P, Marmottant P, Versluis M. Role of the channel geometry on the bubble pinch-off in flow-focusing devices. *Phys Rev Lett*. 2008;100:034504.
40. Garstecki P, Stone H, Whitesides G. Mechanism for flow-rate controlled breakup in confined geometries: a route to monodisperse emulsions. *Phys Rev Lett*. 2005;94:164501.
41. Fu T, Ma Y, Funfschilling D, Li HZ. Bubble formation and breakup mechanism in a microfluidic flow-focusing device. *Chem Eng Sci*. 2009;64:2392–2400.
42. Gordillo J, Sevilla A, Rodríguez-Rodríguez J, Martínez-Bazán C. Axisymmetric bubble pinch-off at high reynolds numbers. *Phys Rev Lett*. 2005;95:194501.
43. Gekle S, Snoeijer J, Lohse D, van der Meer D. Approach to universality in axisymmetric bubble pinch-off. *Phys Rev E*. 2009;80:036305.
44. Eggers J, Fontelos M, Leppinen D, Snoeijer J. Theory of the collapsing axisymmetric cavity. *Phys Rev Lett*. 2007;98:094502.
45. Burton J, Waldrep R, Taborek P. Scaling and instabilities in bubble pinch-off. *Phys Rev Lett*. 2005;94:184502.
46. Eggers J. Nonlinear dynamics and breakup of free-surface flows. *Rev Mod Phys*. 1997;69:865–929.
47. van Hoeve W, Dollet B, Versluis M, Lohse D. Microbubble formation and pinch-off scaling exponent in flow-focusing devices. *Phys Fluids*. 2011;23:092001.
48. Lu Y, Fu T, Zhu C, Ma Y, Li HZ. Pinch-off mechanism for Taylor bubble formation in a microfluidic flow-focusing device. *Microfluidic Nanofluidic*. 2013;16:1047–1055.

*Manuscript received July 8, 2014, and revision received Oct. 16, 2014.*